Wear 477 (2021) 203849

Contents lists available at ScienceDirect

Wear

journal homepage: http://www.elsevier.com/locate/wear

Modeling the effects of individual layer thickness and orientation on the tribocorrosion behavior of Al/Cu nanostructured metallic multilayers

Kaiwen Wang, Wenjun Cai *

Department of Materials Science and Engineering, Virginia Polytechnic Institute and State University, Blacksburg, VA, 24060, USA

ARTICLE INFO

Keywords:
Nanostructured metallic multilayers
Finite element method
Abrasive wear
Tribocorrosion

ABSTRACT

Nanostructured metallic multilayers (NMMs) are emerging materials with excellent mechanical, tribological, and corrosion properties, making them ideal candidates to be used under extremely conditions. The high wear and corrosion resistance lead to enhanced tribocorrosion resistance of NMMs compared to many traditional metals and alloys. In this work, a multiphysics finite element model was developed to study the material deformation and degradation during tribocorrosion from wear, corrosion, as well as their synergy. Specifically, this model accounts for elastic-plastic mechanical deformation during wear and galvanic corrosion between exposed inner layers after wear. The effects of individual layer thickness (from 10 to 100 nm) and layer orientation (horizontally and vertically aligned) on the tribocorrosion behavior of Al/Cu NMMs was studied. Both factors were found to affect the subsurface stress and plastic strain distribution and localized surface corrosion kinetics, hence affecting the overall tribocorrosion rate. This model and the obtained understanding could shed light on future design and optimization strategies of NMMs against tribocorrosion.

1. Introduction

Passive metals such aluminum and titanium alloys, and stainless steels are widely used in marine and offshore industries [1,2], aerospace and transportation [3], and undersea vehicles and infrastructures [4] due to their high strength and corrosion resistance. However, the naturally formed passive layers on these alloys are thin and delicate, leaving the materials vulnerable to mechanical damage, which in turn, jeopardize their resistance to corrosion. This problem is especially prominent during tribocorrosion, where wear and corrosion act synergistically on the surface. Optimization of tribocorrosion resistance usually requires more than that of wear and corrosion resistance alone as numerous experiments indicate that there is typically a tradeoff between wear and corrosion resistance in engineering metals [5]. Hence the optimization of one property might exacerbate the other.

A promising solution of mitigating the wear and corrosion resistance tradeoff lies in an emerging category of materials named nanostructured metallic multilayers (NMMs), where each constituting layer has a thickness of a few to tens of nm. Past research shows that NMMs often exhibit better hardness, wear, and corrosion resistance than their monolithic counterparts [6–10]. For example, Misra et al. synthesized Cu/Nb nanolayers with excellent wear resistance, benefitted from the obstruction of dislocation propagation across the interfaces [11,12]. On the other hand, a research by Fei and Wilcox shows Zn/Ni NMMs exhibit better corrosion resistance than pure Zn and Ni metal due to refined microstructure, decreased surface roughness, and the formation of a more compact and protective oxide film [13]. Although limited research has been conducted on the tribocorrosion resistance of NMMs, these separate wear and corrosion studies indicate great potentials of achieving high tribocorrosion resistance in NMMs.

The individual layer thickness is a key parameter that affects both wear and corrosion resistance of the metallic multilayers. In a research investigating mechanical properties of sputter-deposited Cu–Nb multilayers, Misra et al. [14] report their observation of the strength dependence on layer thickness: the hardness increases as the layer thickness decreases until reaching a maximum at 2 nm; further decreasing the layer thickness leads to a slight drop in hardness. They exploited three different mechanisms including Hall-Petch scaling law, confined layer slip model, and atomistic dislocation transmission, to explain this phenomenon This thickness effect is also observed in Ag/Fe and Ag/Ni multilayer systems by Li et al. [15]. They found that as the layer thickness decreased from a few hundreds to tens of nanometers, both the hardness and wear resistance of the material were improved. As for the corrosion behavior, Flores et al. [16] observed that even though

* Corresponding author.
E-mail address: caiw@vt.edu (W. Cai).

https://doi.org/10.1016/j.wear.2021.203849
Received 14 September 2020; Received in revised form 20 February 2021; Accepted 22 February 2021
Available online 20 March 2021

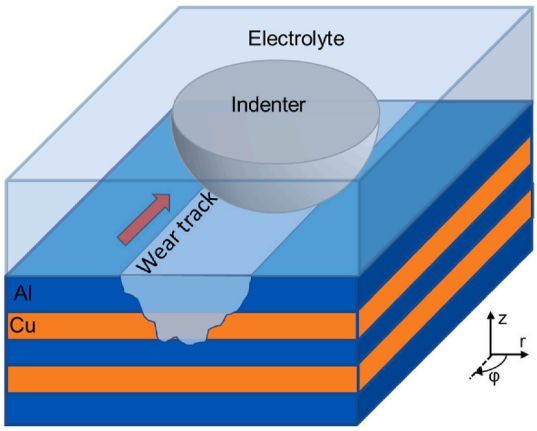

Fig. 1. Schematic of tribocorrosion testing of metallic multilayers used for the FEA model.

reducing the thickness of layers increased the tendency to corrode during the corrosion initialization process, the overall corrosion resistance in long term was improved.

Following these experimental attempts, computational efforts were also made to help better understand the mechanism lays underneath the behavior of metallic multilayers. Finite element analysis (FEA) is a powerful tool in modelling phenomenon caused by this layered structure and capture the state of deformation and degradation within the material. Zhao et al. [17] used FEA to simulate the mechanical response of the TiSiN-based multilayer coating during a nanoindentation test. They explained the formation of the ring, lateral and radial cracks at layer interfaces by analyzing the stress distribution in the multilayer. Mayer et al. [18] investigated the effects of layer orientation and layer waviness on the mechanical behavior of Al–SiC nanolaminate with FEA and further predicted that wavy layers could produce more compliant behavior than flat layers. However, little research has been done so far on simulating tribocorrosion process of metallic multilayers.

This research aims to investigate the effects of layer thickness and orientation on the tribocorrosion behavior of NMMs in 0.6 M NaCl aqueous solution through FEA modeling, using aluminum copper multilayers (Al/Cu) as an example. Al is chosen as it is a widely used passive metal due to its light weight and excellent corrosion resistance. Cu is chosen as a more wear resistant non-passive metal with the same face-centered-cubic (fcc) crystal structure as Al. The outmost layer is assigned to be Al due to its passivity in neutral seawater while the underneath Cu layers provide mechanical support to the structure to maintain its integrity. The model was built to simulate the stress and strain distribution due to wear, the potential and current distribution during corrosion, and predict the time-dependent surface evolution and material removal rate during tribocorrosion. This model provides a numerical framework to probe the mechanical and electrochemical state of NMMs which is hard to obtain through experiments. It also makes the prediction of tribocorrosion induced material degradation of NMMs with different microstructure with great efficiency. The model was verified in terms of mechanical response by Hertzian theory-predicted stress distribution. Finally, the effects of different layer thickness and orientation on the tribocorrosion mechanisms of NMMs were discussed

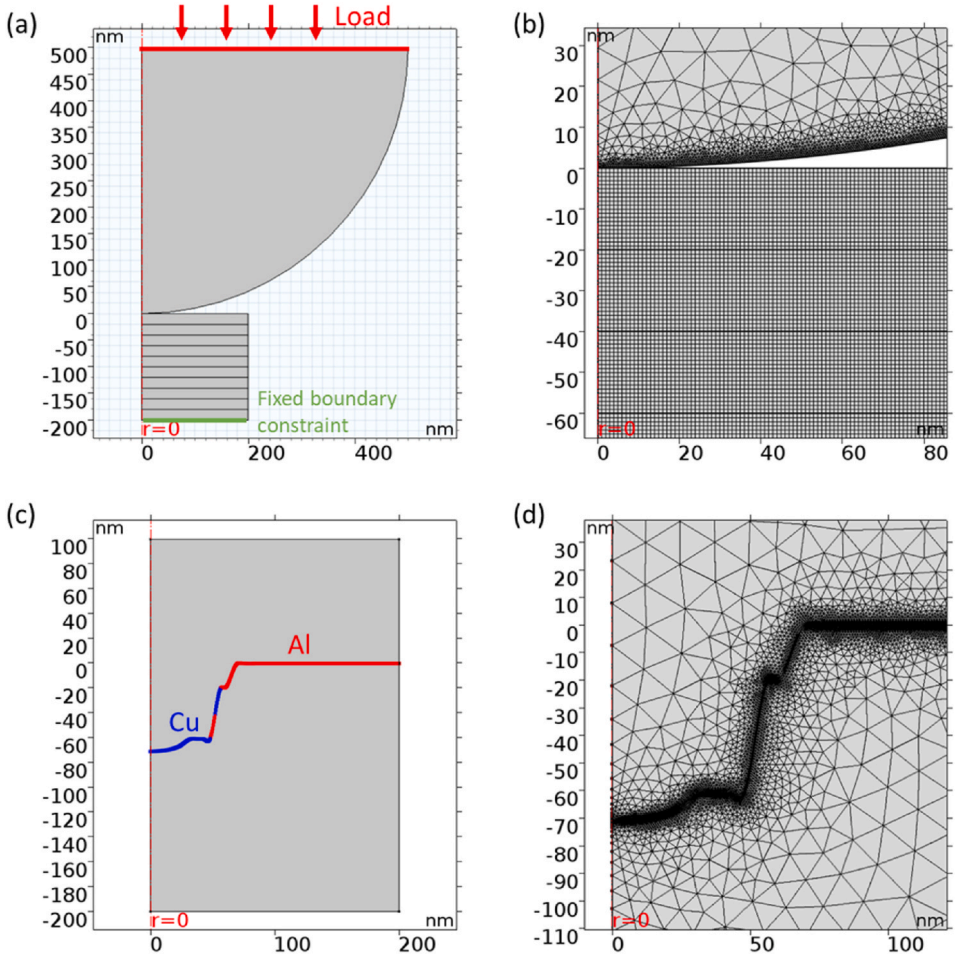

Fig. 2. FEA model of the (a, b) mechanical contact and (c, d) corrosion process geometry setup and meshing.

Table 1
Summary of mechanical parameters of Al and Cu used in the FEA model. E and σ_y represent the Young's modulus and yield strength respectively.

Material	E (GPa)	σ_y (GPa)	ν	Reference
Al	77.62	0.223	0.33	[23]
Cu	117.23	0.330	0.34	[24]
Al_2O_3	300.00	N/A	0.222	[27]

based on these simulation results. These simulation results confirm the recent experimental findings on the superior tribocorrosion resistance of Al/Cu multilayers [19]. The simulation study provided further insights to the underlying mechanism of the improvement in tribocorrosion resistance.

2. Theoretical background and model setup

In this research, a tribocorrosion scenario was investigated where a ball-shaped alumina tip performs a single scratch on the sample surface immersed in 0.6 M NaCl aqueous solution, as shown in Fig. 1. A commercial finite element software COMSOL 5.3 was used and the element removal algorithm was realized with COMSOL Livelink for Matlab. The model involves the solution of a two-body contact problem between the tip and the sample, which causes abrasive wear, and an electrochemical problem of galvanic corrosion between layers of different metals. An axisymmetric 2D geometry setup was employed for computational efficiency. Previous researches have verified with experiments that the stress distribution profile captured by the axisymmetric contact model is sufficient to predict wear volume loss [20–22]. For simplicity, in this model, the total material loss was modeled as a two-step process, where wear proceeded first as a transient state, followed by corrosion of the worn surface.

2.1. Abrasive wear

The geometry of the axisymmetric wear model is shown in Fig. 2 (a). The sample is a 200 × 200 nm square and the counter body is assumed to be a spherical tip with a radius of 0.5 μm. The top layer is Al, followed by Cu. The load was exerted on the top boundary of the indenter while the bottom boundary of the sample was fixed. The sample was meshed in square-shaped elements with an element size of 1 nm while the region near the tip of the indenter is set to be a triangular mesh of 0.5 nm element size, as shown in Fig. 2 (b). The out-of-plane scratch length is 5 mm and the sliding velocity of the indenter is 0.2 mm/s.

The layers were set as linearly-elastic and perfectly-plastic materials, with elastic modulus, Poisson's ratio and yield strength of Al and Cu summarized in Table 1 [23,24]. The plasticity is implemented using the von Mises yield criteria [25,26], which could be generally expressed as

$$F = \sqrt{3J_2} - \sigma_y = 0, \tag{1}$$

where the first term is the von Mises stress, in which $J_2 = \frac{1}{6}((\sigma_{11}-\sigma_{22})^2 + (\sigma_{22}-\sigma_{33})^2 + (\sigma_{33}-\sigma_{11})^2) + \sigma_{12}^2 + \sigma_{23}^2 + \sigma_{13}^2$, and the second term is the yield strength (σ_y). σ_{11}, σ_{22}, σ_{33}, σ_{12}, σ_{13} and σ_{23} are components of stress tensor, where 1, 2, 3 corresponds to x, y, z direction in Cartesian coordinates. In the axisymmetric cylindrical coordinates, the equation could be expressed as $J_2 = \frac{1}{6}((\sigma_r-\sigma_z)^2 + \sigma_r^2 + \sigma_z^2) + \sigma_{rz}^2$, where σ_r and σ_z are normal stress in the r and z direction (as defined in Fig. 1), and σ_{rz} is the shear stress. The strain generated beyond this limit is the effective plastic strain ε_{pl}, which is irrecoverable after the load is removed. The indenter tip was set as a linearly-elastic material with the mechanical property of alumina. The detailed parameters are obtained from COMSOL's built-in database [27] and are also listed in Table 1.

In abrasive wear, materials not only go through plastic deformation referred to as ploughing, which could be calculated using eqn. (1) above, but would also suffer from cutting which accounts for material removal when small debris of material experience highly plastic deformation and detach from the bulk. A wear model with running-in effect based on FEA result and validated by experiments [28] was adopted to simulate the material removal. This algorithm is based on a research by Nélias et al. [29], which claims that material removal would occur when plastic strain exceeds a threshold value and material debris is detached from the surface. This threshold value is affected by many tribological factors including coefficient of friction, surface adhesive force, sliding velocity, and wear cycles, etc. Despite its complexity, this critical plastic strain ε_c could be calibrated using a few rounds of experiments. The acquirement of the precise value of this ε_c is not the main focus of this work, so a sweep through a few representative values of ε_c (from 0 to 0.02) in the wear model was done to demonstrate the model can account for different severity of wear.

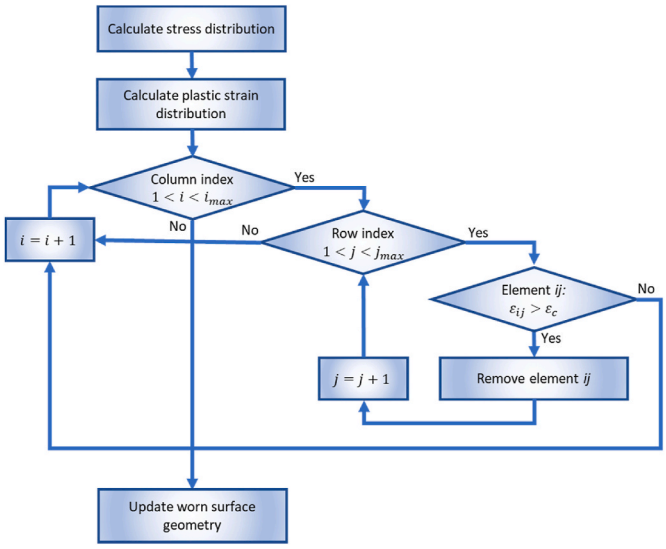

Fig. 3. Flowchart of the algorithm for material removal in the FEA model.

The general algorithm of the wear process is demonstrated in Fig. 3. In this model, first, the FEA simulation was run to calculate the stress and strain distribution of the multilayers. For a given point on the sample surface, starting from the element closest to the surface along the -z direction, ε_{pl} of each element was evaluated. If the obtained ε_{pl} is larger than ε_c, the element is considered as a worn element and removed. The same process was then repeated on the element beneath it until an element with $\varepsilon_{pl} < \varepsilon_c$ was found (unworn element). The element removal operation at this location could then be terminated and the loop proceeds to the next location on the sample surface. The final worn surface is obtained after all surface locations are evaluated using this method.

2.2. Aqueous corrosion

After the wear process is simulated, a corrosive environment is added to the model. Because the electrical conductivity of Al and Cu are both very high, the potential inside the sample will reach an equilibrium of uniform distribution instantly. Thus, the whole sample could be treated as a bulk electrode instead of a layered geometry to avoid convergence issue that could occur in surface evolution when the zigzagged surface intersects with the layer interface. The difference in the corrosion reactions of different layers is achieved by dividing the surface into different sections according to their Z coordinates and assigning the respective reactions, as demonstrated in Fig. 2 (c).

The reaction kinetics at the surface is assumed to follow the Butler-Volmer equation as

Table 2
Summary of electrochemical parameters of Al and Cu used in the FEA model. E_{eq} and i_0 are the equilibrium potential and corrosion current density respectively, and α_a and α_c are the transfer coefficient for the anodic and cathodic reaction respectively.

Material	E_{corr}(V vs. Ag/AgCl)	i_0(A/m^2)	α_a (V/decade)	α_c (V/decade)	Reference
Al	- 0.73	0.0083	0.23	0.23	[30]
Cu	- 0.21	0.012	0.21	0.14	[19]

Table 3
Summary of material parameters of Al and Cu used in Faraday's law.

Material	Electron transferred	**Molar Mass(g/mol)**	ρ (g/cm^3)
Al	3	26.98	2.70
Cu	1	63.55	8.96

$$i_{loc} = i_0\left(\exp\left(\frac{\alpha_a F\eta}{RT}\right) - \exp\left(\frac{-\alpha_c F\eta}{RT}\right)\right), \tag{2}$$

where i_{loc} is the local current density at the electrode surface, i_0 is the exchange current density, α_a and α_c is the transfer coefficient for anodic and cathodic reaction respectively. F, R, T stands for Faraday constant (96485 C/mol), ideal gas constant (R = 8.3145J/(mol·K)) and absolute temperature respectively. The overpotential η is defined as $\eta = -\varphi_l - E_{corr}$, in which φ_l is the electrolyte potential at the sample surface and E_{corr} is the corrosion potential of the metal. E_{corr}. i_0, α_a and α_c (listed in Table 2) are unique electrochemical parameters characterizing the dissolution reaction of Al and Cu and are obtained from Tafel extrapolation of experimentally measured potentiodynamic curves [19,30]. All potentials are converted to the values with respect to an Ag/AgCl reference for all inputs and calculations.

Inside the electrolyte, the current density ($\boldsymbol{i}_l$) and the electrolyte potential (φ_l) satisfy the differential equations of:

$$\begin{cases} \nabla\cdot\boldsymbol{i}_l = Q \\ \boldsymbol{i}_l = -\sigma_l\nabla\varphi_l \end{cases}, \tag{3}$$

where Q stands for the charge sources, which is 0 in the electrolyte in our case, and σ_l is the conductivity of the electrolyte, which is set as 5 S/m as generally measured for sea water.

At the electrolyte/electrode interface, the current density satisfies the boundary condition of $\mathbf{n}\cdot\boldsymbol{i}_l = i_{loc}$ for continuum. The time-dependent electrochemical state of the system was evaluated by solving these differential equations. The material dissolution rate normal to the surface is calculated by taking the current density from above into the Faraday's law:

$$v_n = \frac{i_{loc}M}{nF\rho}, \tag{4}$$

where M is the molar mass, n is the number of electrons transferred in dissolving 1 metal atom, F is the Faraday's constant (96485 C/mol), and ρ is the density of the metal. For the corrosion of Al, the number of electrons transferred is 3. Cu dissolves into a monovalent Cu^+ ion and 1 electron is transferred. The molar mass and density of Al and Cu are listed in Table 3.

Apart from active dissolution, repassivation also occurs on the aluminum surface, during which a layer of thin but dense oxide (mainly Al_2O_3) layer is formed and acts as a barrier to protect the bulk Al. Established theoretical explanation commonly treats this passive layer as a combination of resistance and capacitance in parallel, which is

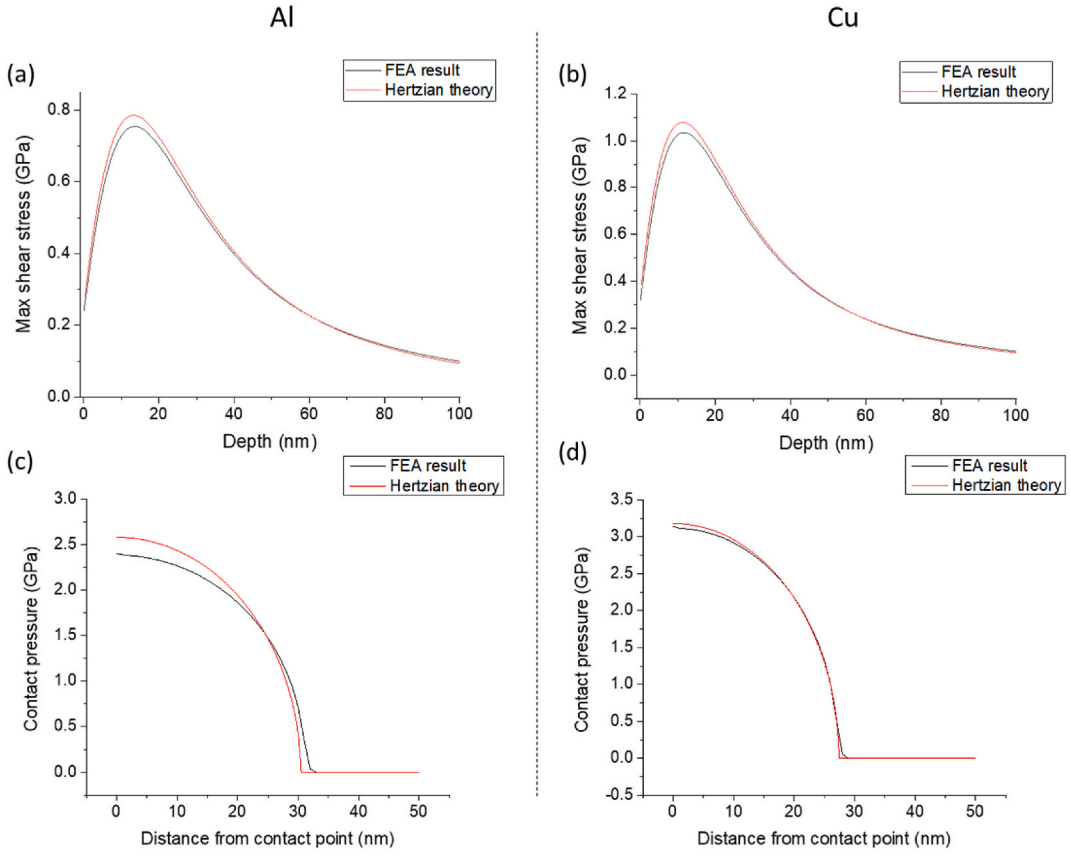

Fig. 4. Comparison between FEA simulation and Hertzian contact theory results: (a, b) maximum shear stress as a function of depth along the loading axis, and (c, d) surface contact pressure as a function of distance from the loading point of Al and Cu.

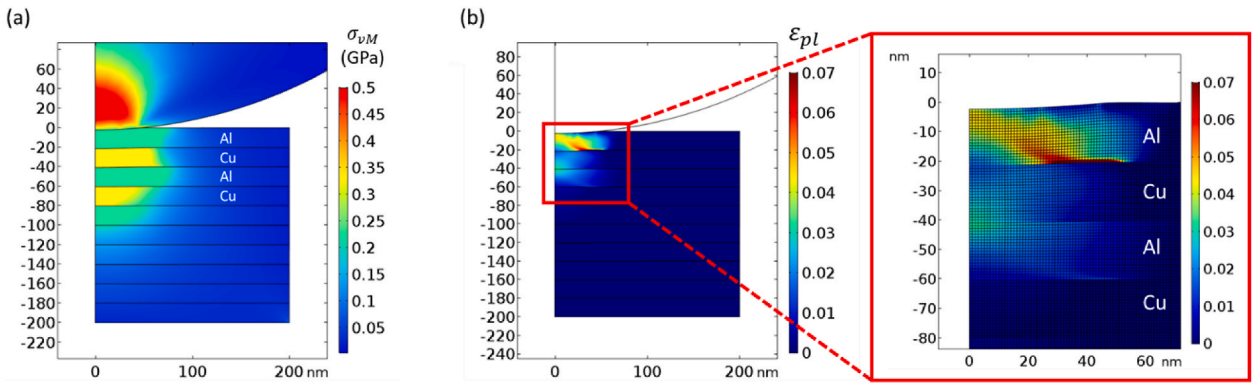

Fig. 5. FEA model predicted (a) von Mises stress and (b) effective plastic strain distribution of Al/Cu NMM under 5 μN load.

justified by electrochemical impedance spectroscopy measurements [31]. In this model, the passive layer is treated as an electrical resistant film whose resistance increases as the film grows thicker. The simulation of the repassivation process was realized using a film resistance option for the electrode surface in COMSOL. Suppose the loss of Al at a location is d in thickness, the accumulated passive layer thickness is $1.29d$ calculated from their molar volume ratio (i.e. M_{Al2O3}/M_{Al}). Along with the dissolution of the Al, the model generates a resistant barrier with local conductivity per unit area of $1.29\sigma d$, where σ is the conductivity of Al_2O_3, which equals to $1 \times 10^{-12} S/m$. For the Al surface outside wear track where the passive layer is intact, a constant film thickness of 4 nm is set, consistent with existing experimental observations [32]. This will significantly reduce the current exchanges between the electrode and electrolyte, simulating the passivation effect. Previous experimental results point out that repassivation of Al typically takes around 1~2 min to complete after tribocorrosion [23,33], so the simulation time for

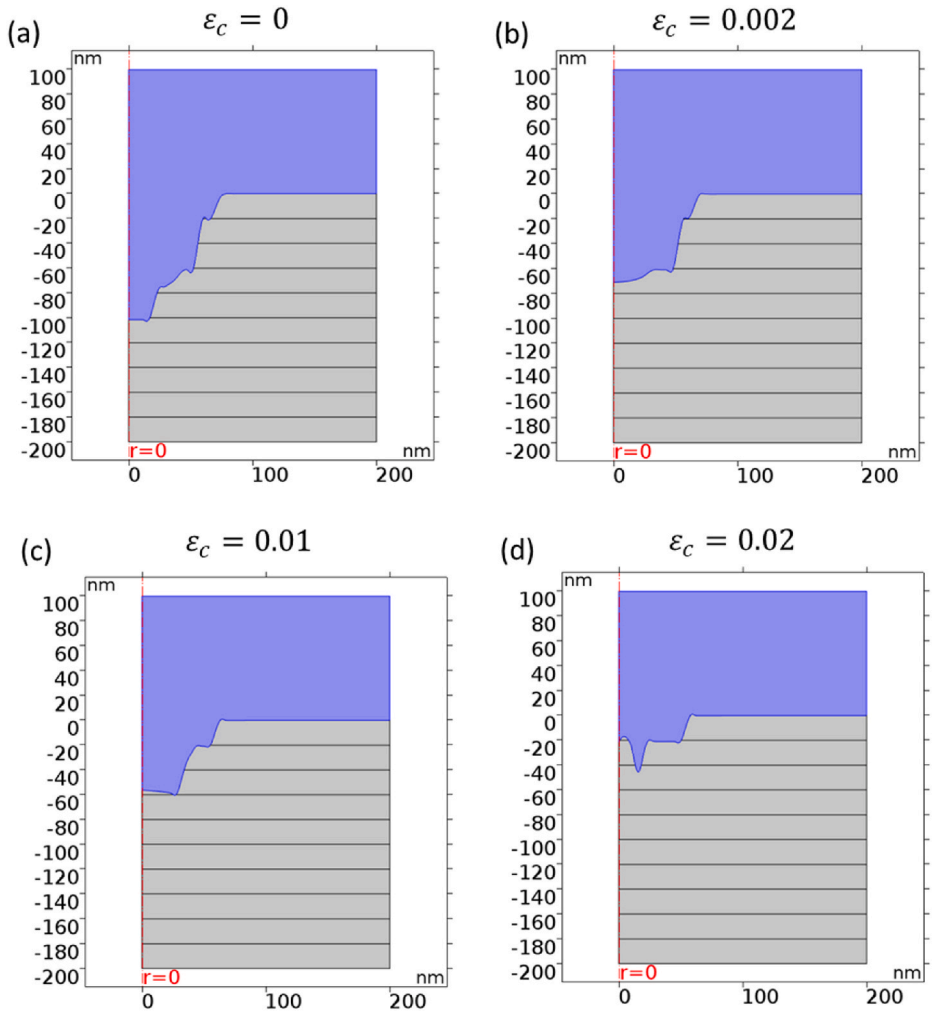

Fig. 6. FEA model predicted worn surface of Al/Cu NMM (h = 20 nm) as a function of critical strain ε_c with value of (a) $\varepsilon_c = 0$, (b) $\varepsilon_c = 0.002$, (c) $\varepsilon_c = 0.01$, and (d) $\varepsilon_c = 0.02$. The blue region denotes the electrolyte. (For interpretation of the references to colour in this figure legend, the reader is referred to the Web version of this article.)

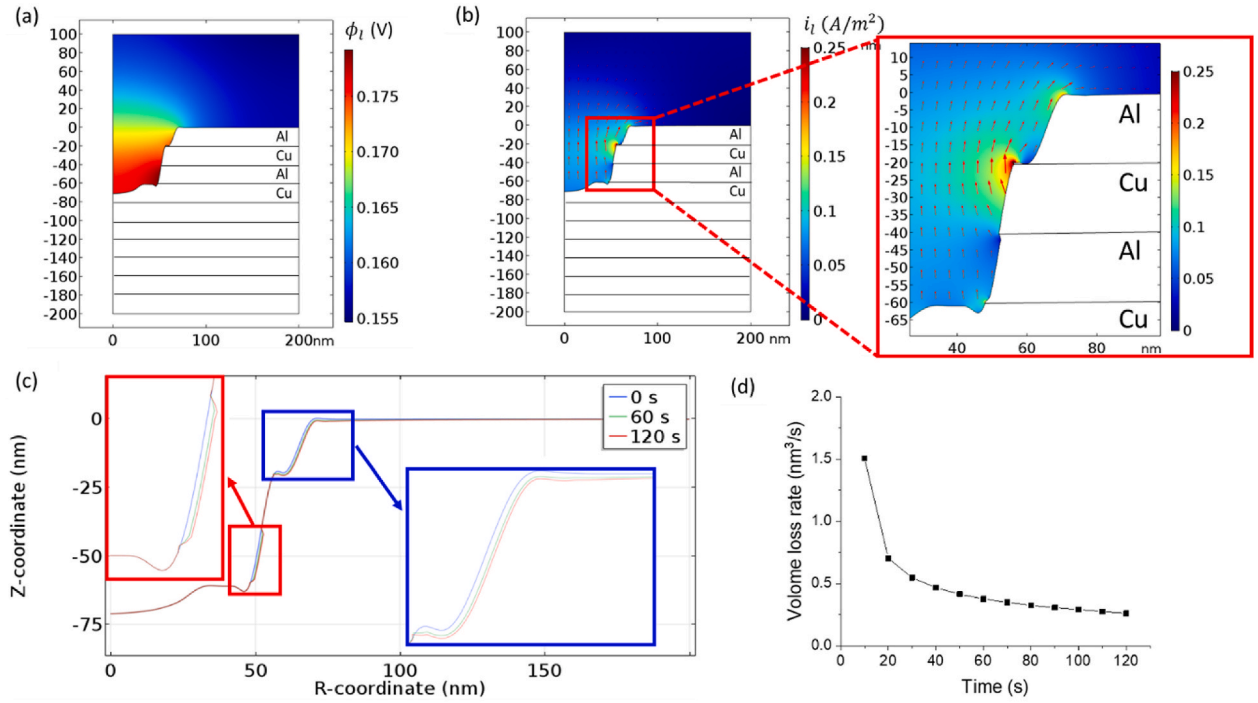

Fig. 7. FEA model predicted (a) electrolyte potential, (b) current density distribution, (c) surface evolution, and (d) total material volume loss due to tribocorrosion as a function of time of Al/Cu NMM (20 nm individual layer thickness) after tribocorrosion process under 5 μN load.

corrosion is controlled to be a total of 120 s with a 10 s timestep. There have been evidences that the corroded Cu in NaCl solutions forms CuCl which is non-adhesive and dissolvable [1,34]. Thus, Cu is treated as active corroding metal with no protective layer. The depassivation/repassivation effects and the galvanic coupling between the exposed inner layers accounts for the synergy between wear and corrosion. Even though some simulation work also involves the change of E_{corr} due to plastic strain to account for synergistic effect [35,36], such method is not applied in this work since it is not compatible with the wear model with the strain-based criterion introduced above. Such effect is considered minor as compared to the synergy caused by depassivation/repassivation and galvanic corrosion. The meshing near the wear track is plotted in Fig. 2 (d). The meshing is set to a finer element size of 1 nm along the sample surface where galvanic coupling between layers is more concentrated and potential gradient is large, while the rest of the model were meshed with coarser elements ranging up to 20 nm. Triangle mesh is used to better accommodate the rugged shape of the surface.

3. Simulation results

3.1. Subsurface deformation and wear

The contact problem of pure bulk materials without considering the plasticity could be verified with analytical solution of Hertzian contact pressure and shear stress. The contact problem of the indenter with monolithic Al and Cu under 5 μN load is studied using both analytical Hertzian contact theory and FEA simulation. As shown in Fig. 4, the result of contact pressure against the distance to the contact point along r axis and maximum shear stress against the depth from the surface along z axis obtained by FEA model is in good agreement with that from the calculation by Hertzian theory, proving the feasibility of using FE model to study wear.

Al/Cu NMMs with an individual layer thickness (h) of 20 nm was chosen to explore the wear mechanism of multilayers. The sample underwent a wear test with an applied normal load of 5 μN from the spherical surface on the top of the tip. Fig. 5 (a) and (b) shows the effective stress and strain distributions across different layers inside the sample respectively when the tip indents the sample. A magnified plot of the contact zone is shown in Fig. 5 (b), which demonstrates the maximum strain occurs within the top Al layer, near the Al/Cu interface. It could be inferred from these results that the Al layers suffers more plastic deformation than their adjacent Cu layers, while the Cu layers carry more load than the softer Al layers. These observations are consistent with those measured experimentally, where layer compression was found to be more significant in the softer layers of Al/Ti and Cu/Ag NMMs [37,38]. The effects of critical strain on the worn surface profile were studied by varying the ε_c values from 0, 0.001, 0.002 and 0.02, which rendered a set of surfaces with different wear severity, as shown in Fig. 6. It can be seen that as the critical strain increases, the overall material loss is reduced. The worn surface depth is generally higher near the loading point (r = 0) and decreases rapidly approaching the edge of the contact area. This overall morphology of worn surface is indeed in good agreement with those observed experimentally on NMMs after indentation and wear tests [39,40]. Due to limited length of the article, for the rest of this work, the case of $\varepsilon_c = 0.002$ was chosen for all tribocorrosion simulations for consistent investigation and discussion.

3.2. Corrosion of the worn surface

Using the worn sample surface generated under 5 μN load, the electrolyte potential and current density distribution during the corrosion of the worn surface was simulated. As shown in Fig. 7, the Al layers, which has lower corrosion potential than Cu, serve as the sacrificial anode locally and protect the exposed Cu surface from corroding. The corrosion current mainly flows from Cu into Al layers. This is similar to the experimental observations in seawater corroded Al–Cu alloys that Cu was preserved on the corroded surface while Al suffers from accelerated corrosion [41]. It is interesting to note that due to the micro-galvanic coupling, the corrosion current near the Al/Cu interfaces is often higher than that far away. In the present case, the highest corrosion current occurs near the interface between the first Al/Cu interface due to the higher surface protrusion from wear.

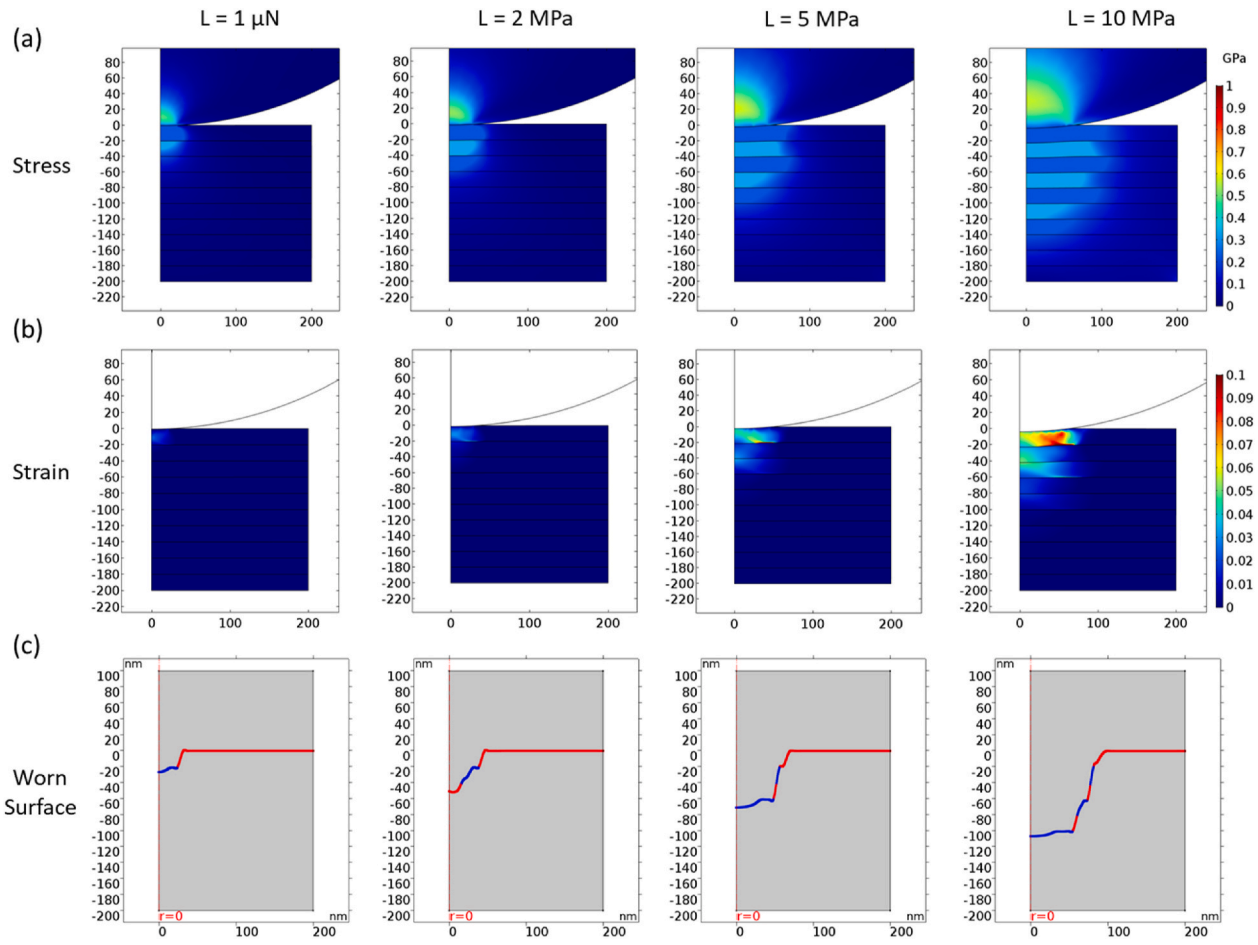

Fig. 8. FEA model predicted (a) stress, (b) strain distribution, and (c) worn surface profile of Al/Cu NMM (20 nm individual layer thickness) under different load L (1–10 μN). The red line denotes the Al layers and the blue line denotes the Cu layers. (For interpretation of the references to colour in this figure legend, the reader is referred to the Web version of this article.)

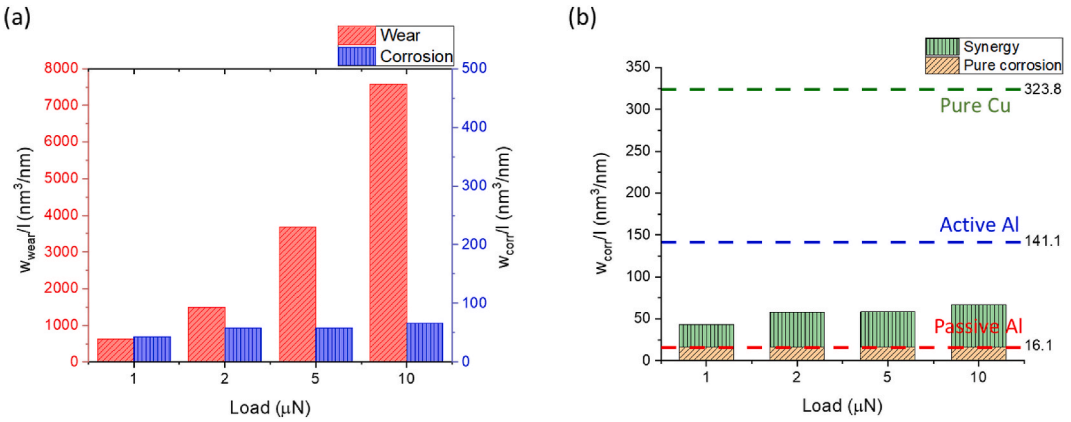

Fig. 9. FEA model predicted (a) material loss rate (i.e. volume loss/sliding distance) due to wear and corrosion process, and (b) material loss rate from wear-corrosion synergy vs. pure corrosion of Al/Cu NMM (20 nm individual layer thickness) under different load. Dashed lines in (b) represent tribocorrosion rate with the same exposed surface area for surface of passive Al (red), active Al (blue), and Cu (green) respectively. (For interpretation of the references to colour in this figure legend, the reader is referred to the Web version of this article.)

The time-dependent evolution of the surface is demonstrated in Fig. 7 (c), which shows that a higher corrosion rate occurs within the Al than the Cu layers. In addition, the overall material loss is higher within the wear track than far away. It should also be noted that the material loss rate is not a constant over time due to repassivation of the Al layers. As shown in Fig. 7 (d), the material loss rate decreases with time, as a result of passive layer's continued growth, making it more effective in limiting the corrosion current flowing through the interface as the (repassivation) time increases.

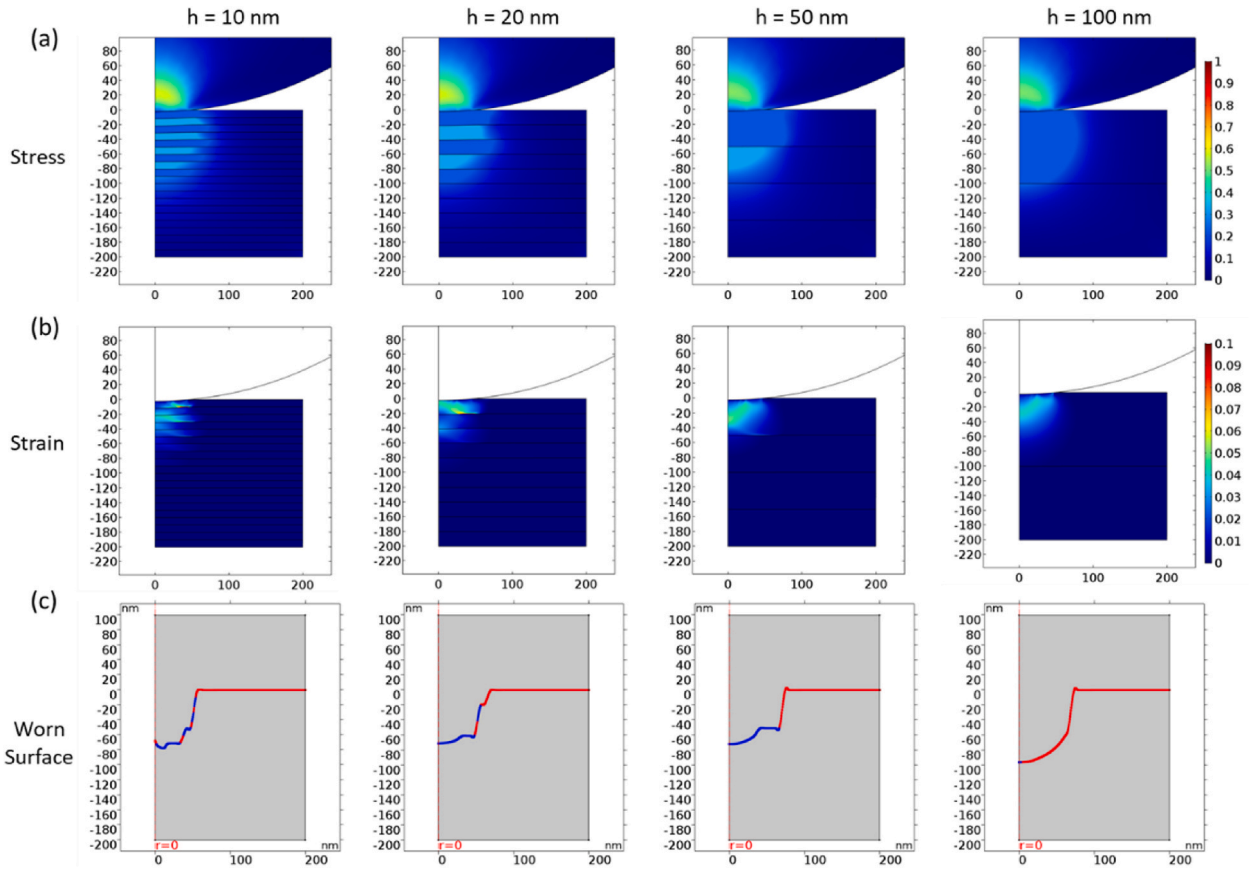

Fig. 10. FEA model predicted (a) stress, (b) strain distribution, and (c) worn surface profile of Al/Cu NMMs with various individual layer thickness h (10–100 nm) under a load of 5 μN.

3.3. Effects of applied load

Fig. 8 shows the mechanical response and worn surface of Al/Cu NMM (h = 20 nm) under different load. As the applied load increases, the contact area and depth of the NMM increases, so are the wear track width and depth. In all cases, the maximum strain occurs within the top Al layer, near the Al/Cu interface. A summary of material loss by wear and corrosion normalized by sliding distance under different load is plotted in Fig. 9 (a). The 2D model simulates the cross-section of the sample and the results for material loss (denoted by w) in all the following graphs are normalized by the sliding distance (l) of the indenter. It is worth noting that even though higher load leads to significantly larger wear track, causing more surface exposure to the corrosive environment, this does not necessarily lead to a significant increase in corrosion rate (Fig. 9(a)). This is mainly because even though the total wear track is broader under higher loads, a large portion of the newly exposed surface is Cu, which almost does not corrode in this process. Here, a wear-corrosion synergy term is defined by the difference between the total corroded volume of the worn surface and that from pure corrosion of the (unworn) NMM, both normalized by the sliding distance. In Fig. 9 (b), the material loss under the same corrosive environment is shown, where the orange and green bar is the material loss rate (volume/sliding distance) caused by pure corrosion and wear-corrosion synergy. The red, blue, green dashed lines represent the theoretical material loss of passive Al, active corroding Al with repassivation effect, and pure Cu respectively under pure corrosive environment. It can be seen that the total tribocorrosion rate of the Al/Cu NMMs falls in between the pure corrosion rate of passive Al and active Al, and significantly lower than that of Cu. This shows that wear-corrosion synergy accelerates corrosion rate and plays an import part in material degradation during tribocorrosion. It also manifests the design of Al/Cu multilayer structure has indeed achieved better tribocorrosion resistance than pure Al and Cu.

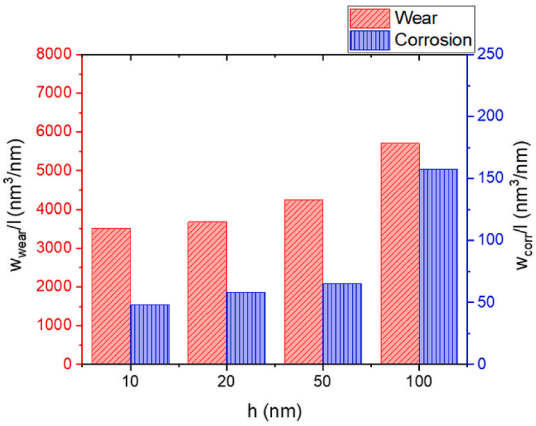

Fig. 11. Summary of FEA model predicted material volume loss rate due to wear and corrosion processes of Al/Cu NMMs as a function of individual layer thickness from 10-100 nm.

3.4. Effects of layer thickness

The FEA model predicted subsurface stress and strain, and the worn surface profile of Al/Cu NMMs as a function of individual layer thickness (h) from 10 nm to 100 nm are shown in Fig. 10. As introduced earlier, the plastic deformation of NMMs when the layer thickness is only a few nanometers involves atomic scale interaction between dislocations and

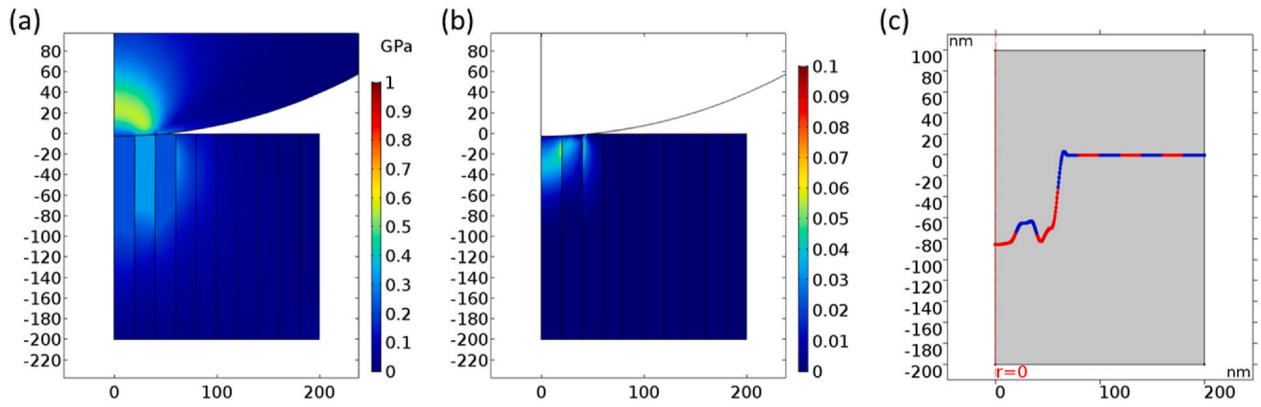

Fig. 12. FEA model predicted (a) stress, (b) strain (b) strain distribution, and (c) worn surface profile of Al/Cu NMMs with vertically aligned layers of 20 nm under a load of 5 μN.

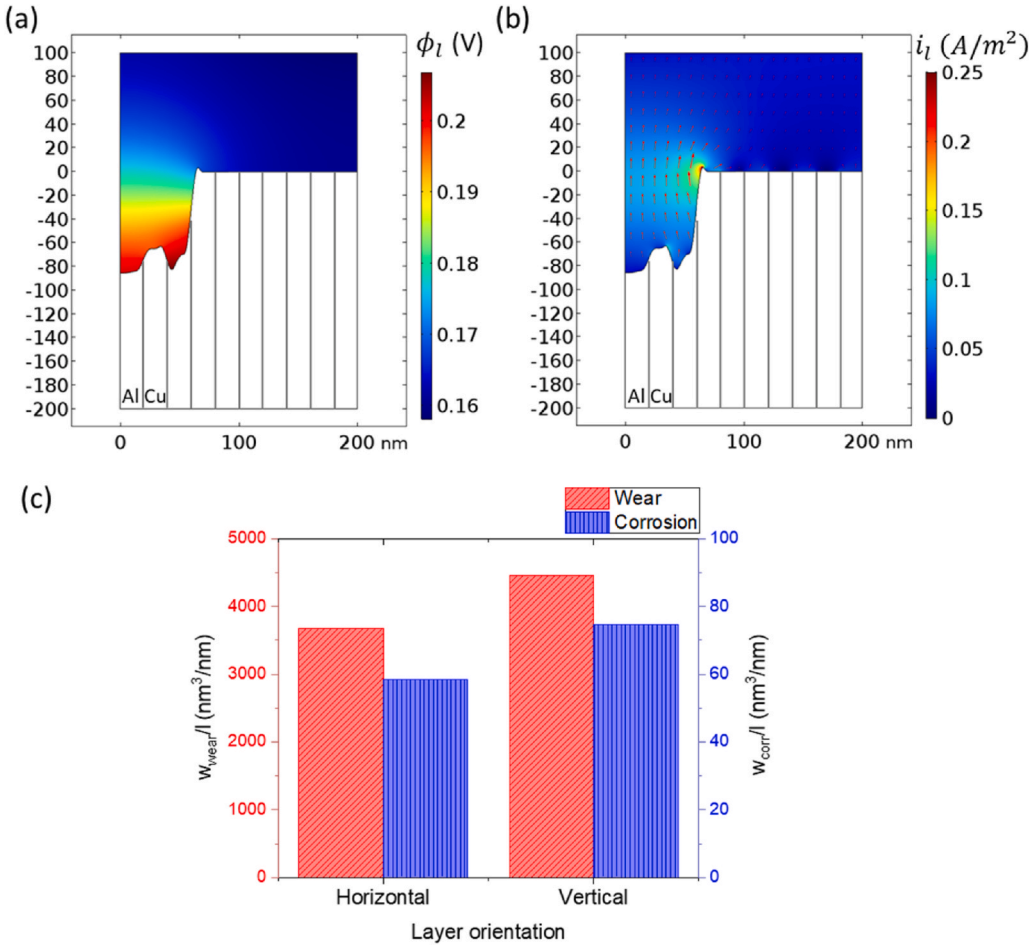

Fig. 13. FEA model predicted (a) electrolyte potential, and (b) current density distribution of Al/Cu NMMs with vertically aligned layers of 20 nm under a load of 5 μN. (c) Summary of material volume loss rate as a function of layer orientation of Al/Cu NMM.

interfaces and could not be modeled by FEA, so extremely small h values (e.g. h < 10 nm) are not considered here where the Hall-Petch breakdown is expected. It could be seen that at finer layers, the buffering effect of Cu layers was increased and the area of material failure was reduced. A more straightforward indication is shown in Fig. 11, which summarizes the material loss caused by wear and corrosion in the tribocorrosion test as a function of layer thickness. Both wear and corrosion resistance of the NMM improves with decreasing layer thickness. This is in good agreement with prior experimental observations [14,37].

3.5. *Effects of layer orientation*

To evaluate the effects of layer (hence interface) orientation, the wear and tribocorrosion behavior of Al/Cu NMM with vertically aligned layers were studied using the FEA model. The individual layer thickness is kept at 20 nm and the load at 5 μN for easy comparison with the prior simulation results. The results are summarized in Figs. 12–13. It could be seen that similar to the horizontal layered NMM, the local strain is higher in the Al layers and stress higher in the Cu layers, especially near

the Al/Cu interfaces. The worn surface morphology is however quite different, where the Al layers wore deeper than Cu layers, leading to significant surface roughness within the wear track (Fig. 12(c)). The difference in the worn surface profile and interface direction lead to different corrosion and tribocorrosion rate. As shown in Fig. 13, the galvanic coupling for vertical layered NMM is more intense, causing a higher corrosion rate than horizontal layered NMMs.

4. Discussion

From the simulation results of wear, it could be inferred that Cu layers experience lower plastic strain than Al layers due to their higher yield strength that helps buffer the yielding of the NMM. This causes significant difference at the edge of wear area since Cu layer may offer protection to the Al layer underneath, preventing material degradation at local areas where Al has already given in. On the other hand, the Al layers act as a sacrificial anode to protect Cu layer from corrosion. Even though this accelerates the dissolution of Al at the beginning, the current interchange between Al and Cu layers helps the repassivation process as time increases. The NMM system quickly reaches a steady state where Cu doesn't corrode and the corrosion rate of Al is reduced to a very small value. All together, these layered structure lead to the better wear resistance of Al/Cu NMM than pure Al and better tribocorrosion resistance than both Al and Cu.

In terms of layer thickness effect, thinner layers allow a denser arrangement of Cu layers preventing debris formation and material loss, which leads to shallower and narrower wear tracks. Despite the fact that the FEA model didn't account for atomic interactions at layer interfaces and nanoscale dislocation propagations, the model suggests that this structural effect could partially explain the mechanical properties' dependence on layer thickness of the multilayers. In corrosion, thinner layers lead to more concentrated current exchange between the layers. This enhance the cathodic protection of Cu layers as well as promoting the formation of passive layer at exposed Al layers. This also resembles the experimental observation in intergranular corrosion of Al–Cu alloy [42].

Finally, the FEA model predicts a significant effect of layer orientation on the overall tribocorrosion behavior of NMMs. In the case of vertical layers, deeper material loss was found in the softer Al layers, eventually resulting in higher volume loss from both wear and corrosion process. On the other hand, in parallel layered NMM, Cu layers block the material removal and help sustain the integrity of the layers underneath. This also leads to less exposure of depassivated Al surface area, causing a less severe anodic corrosion of the Al layers and faster repassivation process. Thus, the integrity of vertically aligned multilayers is more likely to be threatened by tribocorrosion than the horizontally aligned multilayers. As a last note, it is worth pointing out that the current simulation treated the surfaces of both indenter and sample as ideally smooth in geometry and did not take contacting asperities into account. For example, Ghanbarzadeh et al. developed an asperity-scale mechanistic model to investigate the influence of surface asperities on wear-corrosion synergy [43]. More accurate treatment of surface contact between the Al/Cu multilayers and the counter body requires systematic characterization of the real contact area experimentally, which is left for future work.

5. Conclusions

In this research, a finite element model incorporated with an element removal algorithm is developed to investigate the wear and corrosion in the tribocorrosion process of Al/Cu nanostructured metallic multilayers. The mechanical module of the model was used to simulate the structural interaction between layers and predict the stress, strain distribution as well as the wear track morphology. The electrochemical module of the model takes dynamic process of galvanic corrosion between layers and repassivation of the passive metal layers into account and simulates potential distribution, current density and surface evolution of the corrosion process near the wear track. The developed model was used to study the tribocorrosion of Al/Cu multilayers of different layer thicknesses and orientation under different loading conditions. Key findings include:

(1). The combination of a wear resistant cathodic metal (Cu) and an anodic metal with passive layer (Al) lead to improved tribocorrosion resistance than their monolithic counterparts;
(2). Thinner layer thickness (within the range of 10∼100 nm) leads to enhanced wear and tribocorrosion resistance in NMMs;
(3). Multilayers with layer orientation perpendicular to the surface suffers more severe tribocorrosion than those with parallel arrangement.

The developed model could potentially be extended to investigate tribocorrosion performance of metals and coatings with other complex microstructure (e.g. eutectic structure, dual phase, precipitates of various shape, size, and orientation) under a wide range of loading and corrosion conditions.

Credit author statement

Kaiwen Wang: Investigation; Software; Validation; Writing – original draft. Wenjun Cai: Funding acquisition; Conceptualization; Supervision; Writing – review & editing.

Declaration of competing interest

The authors declare that they have no known competing financial interests or personal relationships that could have appeared to influence the work reported in this paper.

Acknowledgements

This research was financially supported by the US National Science Foundation DMR-1856196 and CMMI-1855651. The computational resource used in this work is provided by the advanced research computing at Virginia Polytechnic Institute and State University.

Appendix A. Supplementary data

Supplementary data to this article can be found online at https://doi.org/10.1016/j.wear.2021.203849.

References

[1] T. Liu, S.G. Chen, S. Cheng, J.T. Tian, X.T. Chang, Y.S. Yin, Corrosion behavior of super-hydrophobic surface on copper in seawater, Electrochim. Acta 52 (28) (2007) 8003–8007.
[2] S. Roy, J.M. Coyne, J.A. Novak, M.A. Edwards, Flow-induced failure mechanisms of copper pipe in potable water systems, Corrosion Rev. 36 (5) (2018) 449–481.
[3] R.L. Twite, G.P. Bierwagen, Review of alternatives to chromate for corrosion protection of aluminum aerospace alloys, Prog. Org. Coating 33 (2) (1998) 91–100.
[4] Y.S. Kim, S.K. Lee, H.J. Chung, J.G. Kim, Influence of a simulated deep sea condition on the cathodic protection and electric field of an underwater vehicle, Ocean. Eng. 148 (2018) 223–233.
[5] D.D. Macdonald, Passivity - the key to our metals-based civilization, Pure Appl. Chem. 71 (6) (1999) 951–978.
[6] G.S. Was, T. Foecke, Deformation and fracture in microlaminates, Thin Solid Films 286 (1–2) (1996) 1–31.
[7] K.O. Schweitz, J. Chevallier, J. Bottiger, W. Matz, N. Schell, Hardness in Ag/Ni, Au/Ni and Cu/Ni multilayers, Philos. Mag. A 81 (8) (2001) 2021–2032.
[8] J. Creus, E.H. Top, C. Savall, P. Refait, C. Ducros, F. Sanchette, Mechanical and corrosion properties of dc magnetron sputtered Al/Cr multilayers, Surf. Coating. Technol. 202 (16) (2008) 4047–4055.
[9] T.T. Xie, S.D. Mao, C. Yu, S.J. Wang, Z.L. Song, Structure, corrosion, and hardness properties of Ti/Al multilayers coated on NdFeB by magnetron sputtering, Vacuum 86 (10) (2012) 1583–1588.
[10] S. Izadi, H. Mraied, W.J. Cai, Tribological and mechanical behavior of nanostructured Al/Ti multilayers, Surf. Coating. Technol. 275 (2015) 374–383.

[11] R.G. Hoagland, J.P. Hirth, A. Misra, On the role of weak interfaces in blocking slip in nanoscale layered composites, Philos. Mag. A 86 (23) (2006) 3537–3558.
[12] N.A. Mara, D. Bhattacharyya, P. Dickerson, R.G. Hoagland, A. Misra, Deformability of ultrahigh strength 5 nm Cu/Nb nanolayered composites, Appl. Phys. Lett. 92 (23) (2008).
[13] J.Y. Fei, G.D. Wilcox, Electrodeposition of zinc-nickel compositionally modulated multilayer coatings and their corrosion behaviours, Surf. Coating. Technol. 200 (11) (2006) 3533–3539.
[14] A. Misra, J.P. Hirth, R.G. Hoagland, Length-scale-dependent deformation mechanisms in incoherent metallic multilayered composites, Acta Mater. 53 (18) (2005) 4817–4824.
[15] J. Li, Y. Chen, S. Xue, H. Wang, X. Zhang, Comparison of size dependent strengthening mechanisms in Ag/Fe and Ag/Ni multilayers, Acta Mater. 114 (2016) 154–163.
[16] M. Flores, S. Muhl, L. Huerta, E. Andrade, The influence of the period size on the corrosion and the wear abrasion resistance of TiN/Ti multilayers, Surf. Coating. Technol. 200 (5–6) (2005) 1315–1319.
[17] X.L. Zhao, Z.H. Xie, P. Munroe, Nanoindentation of hard multilayer coatings: finite element modelling, Mater. Sci. Eng. A Struct. 528 (3) (2011) 1111–1116.
[18] C. Mayer, L.W. Yang, S.S. Singh, H. Xie, Y.L. Shen, J. Llorca, J. Molina-Aldareguia, N. Chawla, Orientation dependence of indentation behavior in Al-SiC nanolaminate composites, Mater. Lett. 168 (2016) 129–133.
[19] W. Wang, K. Wang, Z. Zhang, J. Chen, T. Mou, F.M. Michel, H. Xin, W. Cai, Ultrahigh tribocorrosion resistance of metals enabled by nano-layering, Acta Mater. 206 (2021).
[20] J. Ding, I.R. McColl, S.B. Leen, P.H. Shipway, A finite element based approach to simulating the effects of debris on fretting wear, Wear 263 (2007) 481–491.
[21] V. Hegadekatte, N. Huber, O. Kraft, Finite element based simulation of dry sliding wear, Model Simul. Mater. Sci. 13 (1) (2005) 57–75.
[22] P. Podra, S. Andersson, Simulating sliding wear with finite element method, Tribol. Int. 32 (2) (1999) 71–81.
[23] H. Mraied, W.J. Cai, The effects of Mn concentration on the tribocorrosion resistance of Al-Mn alloys, Wear 380–381 (2017) 191–202.
[24] M. Hommel, O. Kraft, E. Arzt, A new method to study cyclic deformation of thin films in tension and compression, J. Mater. Res. 14 (6) (1999) 2373–2376.
[25] A. Akchurin, R. Bosman, P.M. Lugt, A stress-criterion-based model for the prediction of the size of wear particles in boundary lubricated contacts, Tribol. Lett. 64 (3) (2016).
[26] M. Woldman, E. Van der Heide, T. Tinga, M.A. Masen, A finite element approach to modeling abrasive wear modes, Tribol. Trans. 60 (4) (2017) 711–718.
[27] C. Multiphysics, Structural Mechanics Module, User's Guide, Ver 5.3.
[28] R. Bosman, D.J. Schipper, Transition from mild to severe wear including running in effects, Wear 270 (7–8) (2011) 472–478.
[29] D. Nelias, V. Boucly, M. Brunet, Elastic-plastic contact between rough surfaces: proposal for a wear or running-in model, J. Tribol. Trans. ASME 128 (2) (2006) 236–244.
[30] H. Mraied, W.J. Cai, A.A. Sagues, Corrosion resistance of Al and Al-Mn thin films, Thin Solid Films 615 (2016) 391–401.
[31] F. Mansfeld, S. Lin, S. Kim, H. Shih, Pitting and passivation of Al-alloys and Al-based metal matrix composites, J. Electrochem. Soc. 137 (1) (1990) 78–82.
[32] Y.S. Tak, K.R. Hebert, Initial events during the passivation of rapidly dissolving aluminum surfaces, J. Electrochem. Soc. 141 (6) (1994) 1453–1459.
[33] D. Chidambaram, C.R. Clayton, G.P. Halada, Studies on the repassivation behavior of aluminum exposed to dichromate solution, Electrochem. Soc. 2001 (5) (2001) 282–289.
[34] K.F. Khaled, Studies of the corrosion inhibition of copper in sodium chloride solutions using chemical and electrochemical measurements (vol 125, pg 427, 2011), Mater. Chem. Phys. 130 (3) (2011) 1394–1395.
[35] K.W. Wang, Y.N. Wang, X.W. Yue, W.J. Cai, Multiphysics modeling and uncertainty quantification of tribocorrosion in aluminum alloys, Corrosion Sci. 178 (2021).
[36] L.Y. Xu, Y.F. Cheng, Development of a finite element model for simulation and prediction of mechanoelectrochemical effect of pipeline corrosion, Corrosion Sci. 73 (2013) 150–160.
[37] S.P. Wen, R. Zong, F. Zeng, Y. Gao, F. Pan, Investigation of the wear behaviors of Ag/Cu multilayers by nanoscratch, Wear 265 (11–12) (2008) 1808–1813.
[38] K.K. Fu, L. Chang, C.H. Yang, L. Sheppard, H.J. Wang, M. Maandal, L. Ye, Plastic behaviour of high-strength lightweight Al/Ti multilayered films, J. Mater. Sci. 52 (24) (2017) 13956–13965.
[39] M. Berger, U. Wiklund, M. Eriksson, H. Engqvist, S. Jacobson, The multilayer effect in abrasion - optimising the combination of hard and tough phases, Surf. Coating. Technol. 116 (1999) 1138–1144.
[40] K.K. Fu, L. Sheppard, L. Chang, X.H. An, C.H. Yang, L. Ye, Comparative study on plasticity and fracture behaviour of Ti/Al multilayers, Tribol. Int. 126 (2018) 344–351.
[41] W.A. Badawy, F.M. Al-Kharafi, A.S. El-Azab, Electrochemical behaviour and corrosion inhibition of Al, Al-6061 and Al-Cu in neutral aqueous solutions, Corrosion Sci. 41 (4) (1999) 709–727.
[42] J.R. Galvele, S.M. Demicheli, Mechanism of intergranular corrosion of Al-Cu alloys, Corrosion Sci. 10 (11) (1970) 795–+.
[43] A. Ghanbarzadeh, F.M. Salehi, M. Bryant, A. Neville, A new asperity-scale mechanistic model of tribocorrosive wear: synergistic effects of mechanical wear and corrosion, J. Tribol. 141 (2) (2019).